RESEARCH PAPER

Inherent radiological hazard and γ-ray shielding properties of black sand minerals

Tamer G. Mohamed [a,b,*], Mostafa Hassan [c], Ayman A. El-Midany [b], Mohamed A. Ismail [b], Moamen G. El-Samrah [d]

[a] Training Department, Engineering Authority, Armed Forces, Cairo, Egypt
[b] Department of Mining and Geological Engineering, Faculty of Engineering, Cairo University, Egypt
[c] Department of Civil Engineering, Military Technical College, Cairo, Egypt
[d] Department of Nuclear Engineering, Military Technical College, Cairo, Egypt

Abstract

In this study, seven mineral products derived from Egyptian black sands were studied to assess the feasibility of using them in γ-ray shielding materials. These mineral products, along with their assigned codes are zircon, ilmenite grade no. 1 (ilmenite#1), black sand concentrate, magnetite, green silica, rutile, and ilmenite grade no. 2 (ilmenite#2). During this study, the studied samples have been characterized to identify their compositions, particle size, and real densities. Then, the activity concentrations considering the naturally occurring radioactive nuclides were experimentally determined, and then the most important radiological hazard indices were calculated and evaluated. Finally, the radiation shielding properties of the eligible minerals have been assessed. Based on the performed experimental and analytical programs, four products were found to be eligible for preparing radiation shielding building materials considering that magnetite and ilmenite were found the best among the studied samples.

Keywords: Egyptian black sands, Hazard indices, Mineral products, Naturally occurring radioactive materials, γ-ray shielding

1. Introduction

In this era, nuclear and radiological applications play a vital role in almost all facets of industrial and medical affairs. For instance, the growing number of nuclear power plants, radiological medical facilities, and nuclear research facilities have raised the importance of protection and shielding against various types of radiation.[1,2] As a logical consequence, searching for effective feasible shielding materials has become unstoppable.

Many studies have focused on the preparation and assessment of radiation shielding materials such as modified glass systems incorporating nanoparticles such as bismuth oxide, barium oxide, and boron tellurites,[3–5] polymeric composites modified by inorganic fillers and heavy metal oxides,[6,7] alloys such as high-density iron–copper alloy, iron–boron, and cerrobend alloys,[8–10] and improved building materials such as fiber-reinforced hematite concrete, high-performance concrete with special aggregates such as goethite, limonite, barite, and steel slag, and modified bricks that contained nano-bentonite.[11–15] However, obtaining proper building materials including bricks, cementitious mortars, and modified concrete with enhanced radiation shielding properties has the lion's share of the total experimental and analytical studies in this research field as building materials are considered the cornerstone of all nuclear constructional applications.[1,16,17]

To save costs, area, and at the same time obtain improved radiation shielding properties, certain untraditional additives/aggregates have been

Received 11 September 2023; revised 5 June 2024; accepted 9 June 2024.
Available online 29 July 2024

* Corresponding author.
E-mail address: gadtamer02@gmail.com (T.G. Mohamed).

https://doi.org/10.62593/2090-2468.1036

intensively studied to investigate their effects not only on the radiation shielding capability of the studied building materials but also on their physical and mechanical properties.[1,16,17] Working on the overall properties of the shield is crucial to get a proper radiation shield; however, obtaining a shield with ideal comprehensive characteristics is something that seems unreal; thus, optimization based on the intended application is the right action.[1,2,18]

Black sands and their attributed minerals such as ilmenite, magnetite, garnet, zircon, rutile, monazite, etc., have also been found very attractive to investigate their radiation shielding capabilities especially against energetic photons, that is, radiographs and γ-rays, as they usually contain appreciated amounts of high-Z elements such as titanium, iron, zirconium, lanthanum, cerium, thorium, and uranium.

Egyptian black sands specifically, which are located at specific spots along the Mediterranean Sea coast as shown in Fig. 1 are rich in certain minerals such as ilmenite, magnetite, rutile, green silica, zircon, and monazite. All of these minerals upon separation were found to possess high densities and considerable high-Z element contents that nominate them to own promising radiation shielding properties and that was a motivating factor to initiate the current study.

Despite all of the former, radiological hazard assessment of the probable additives and aggregates, especially those with sedimental, oolitic, and soil-related origin, has not been given the required attention through most of the formerly denoted studies before electing them for employment in radiation shields. Some of those exceptional materials, especially mineralogical products separated from black sands, that can be used in the production of building materials with improved radiation shielding properties, may contain significant concentrations of natural radioisotopes, which are called naturally occurring radioactive materials (NORMs).[19,20]

The radiological hazard of these materials/minerals arises from two sources; the first one is the possible increase in the external received dose that mostly comes from ^{238}U and ^{232}Th and their progenies along with ^{40}K. The second highly appreciated source is the increased internal radiation dose that comes mainly due to radon, ^{222}Rn, and exhalation from buildings constructed based on these materials especially when these buildings are closed and improperly ventilated.[20–22] Radon, which is a hazardous alpha emitter, can easily enter the human respiratory system and cause serious damage that may lead eventually to lung cancer.[20,23]

Based on the former, besides the importance of getting an effective radiation shield with optimized physical and mechanical properties, the possible radiological hazards that may arise from the materials that comprise the shield must be assessed especially if the shield is planned to be used in residential and working places.[20,22]

Fig. 1. Black sand-rich regions near areas of Rasheed and El-Burullus (satellite picture obtained from Google Maps).

Through this study, representative samples for seven products obtained from The Black Sand Company in Egypt were investigated. The study was conducted in three phases. First, the characterization of the investigated samples using radiograph fluorescence (XRF) to define their chemical composition besides measuring their real density and average particle size. Second, the assessment of the radiological hazard of these samples is undertaken by measuring the activity concentrations of their content of the NORMs and estimating some important associated radiological hazard indices. The last and principal phase is investigating the radiation shielding properties of the eligible minerals, based on the results obtained from the second phase, against energetic photons at selective energies and extracting the most important shielding parameters to assess the feasibility of using these products in manufacturing building materials with improved radiation shielding capabilities, especially against radiographs and γ-rays.

2. Materials and methods

2.1. Materials

The studied samples were taken as representative samples for seven products obtained from The Black Sand Company in Egypt. First, it should be noted that the Egyptian black sand, that are located on the northern coast, especially near the areas of El-Burullus and Rasheed, is rich in considerable concentrations of economic minerals as denoted before along with some radioactive elements in concentrations higher than the ordinary global level.[24,25] The indicated seven products are zircon, ilmenite grade no. 1 (ilmenite#1), black sand concentrate (BSC), magnetite, green silica, rutile, and ilmenite grade no. 2 (ilmenite#2). They are all extracted from black sand after performing specific mechanical, magnetic, and electrostatic separations.[26,27] The flowchart describing the separation stages and the output weight percentages of the separated products is shown in Fig. 2.

The final obtained mineral percentages are 40, 15, 15, 10, and 20% for ilmenite (grades 1 and 2), magnetite, zircon, rutile, and other mineral products such as green silica, garnet, and monazite.

As mentioned earlier, those mineralogical products have certain economic feasibility. For example, zircon is usually used in the ceramics industry; besides, it contains zirconium, which is used in nuclear fuel rods manufacturing. Ilmenite and rutile are significant sources of titanium which is highly resistant to aggressive environments that comprise high temperatures, urban pollution, and/or corrosive compounds. So, it is usually used with other metals to manufacture high-performance alloys which can be used in such industrial environments such as aerospace applications, jet engine

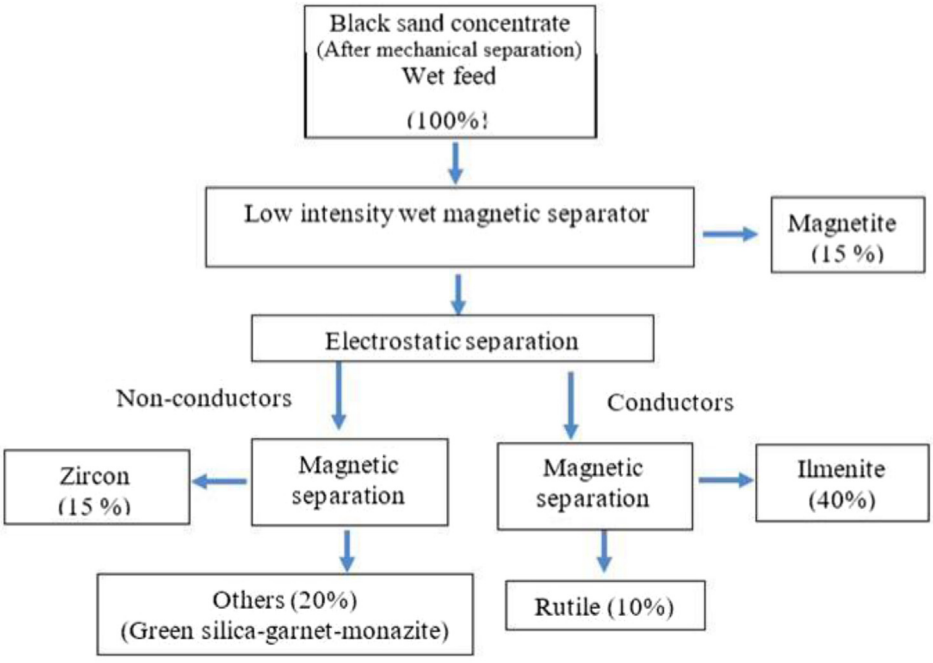

Fig. 2. Schematic flow sheet for Egyptian black sand separation steps along with the obtained mineralogical products.

manufacturing, and airframes. Moreover, magnetite, which is an important iron ore, is widely used in the sponge iron industry and for oil pipe wrapping. Last but not least, monazite, is a valuable ore from which thorium and many rare earth elements can be extracted. Nevertheless, in this study, we focus on the feasibility of these mineral products for use as additives or alternatives to obtain building materials with improved radiation shielding capabilities.[25,28]

2.2. Methods

2.2.1. Characterization of the investigated materials

2.2.1.1. Chemical composition determination using the XRF technique. XRF is a nondestructive analyzing technique that depends on the emission of characteristic (fluorescent) radiographs from a material that has been excited after the bombardment with energetic radiographs. This phenomenon/technique is widely used to define the chemical composition, particularly during the characterization of alloys, ceramics, glass, ores, and building materials. The studied samples were analyzed to get their chemical composition using the S-8 Tiger Bruker XRF Spectrometer from Bruker, Karlsruhe, Germany.[29]

2.2.1.2. Real density measurement. The real density of the investigated samples was measured using Ultrapyc 1200e Automatic Gas Pycnometer from Quantachrome Instruments, USA. The Ultrapyc 1200e Automatic Gas Pycnometer, P/n 02112-1, is used for measuring the actual density and solids' volume through an automatic process. An appropriate expansion volume is automatically chosen by the microprocessor according to the selected sample cell. The system resolution is 0.0001 g/cm^3 and the used gas is highly-purified nitrogen gas.

2.2.1.3. Particle size analysis. Particle size distribution and average particle size of the investigated samples were obtained using a BT-2001 particle size analyzer which uses a laser diffraction technique. It is a dispersing system that adopts the Venturi dispersing effect by measuring shear, inertia, collision, etc., to guarantee that the analyzed powder is in a complete dispersing state while passing through the testing zone.[30] The system includes a large-size photodetector array along with a large-scale integrated circuit that provides higher analyzing sensitivity, accuracy, and resolution. The used dispersive medium is water with an index of 1.33 and the detection range is between 0.1 and 1036 μm.

2.2.2. Radiological activity measurements and associated hazard indices

2.2.2.1. Specific radioactivity measurements. Representative samples were taken for the seven mineral products under investigation. All the samples were in microscale and homogenized, so there was no need for further sieving through a fine mesh. The samples were dried at 100 °C in a tightly sealed oven for 24 h to remove the contained moisture. After that, the selected samples were put in polyethylene Marinelli containers with a standard geometry that has a volume of 212.6 cm^3. The containers were tightly sealed and left for 28 days before the radiological activity measurements just to reach secular equilibrium between ^{226}Ra (represents ^{238}U decay chain), ^{232}Th, and their daughters.[20,31]

The radiological activity measurements were held using a sodium iodide (NaI (Tl)) scintillation detector (Bicron) with a 3′ × 3′ crystal hermetically sealed with a photomultiplier tube in an aluminum housing. To protect against induced radiographs and background radiation, the detector is placed in a cylindrical hollowed lead chamber with a copper internal liner that has a thickness of 6 mm, and a "5 cm" lead lid is put over just after placing the sample that will be measured.

Before starting the measurements, an energy calibration was carried out using precisely calibrated radioactive standard sources and then, efficiency calibration was performed using four geological reference materials prepared from a series of certified reference samples with certain ^{226}Ra, ^{232}Th, and ^{40}K activity concentrations obtained from the International Atomic Energy Agency. The former energy and efficiency calibrations are necessary to ensure that the NORM activities to be measured are taken accurately at the chosen gamma radiation energies.

Uranium and thorium are alpha, not gamma, emitters, so they are indirectly measured using specific gamma lines emitted by their daughters.[31] Radioactivity of ^{226}Ra, ^{232}Th, and ^{40}K was measured using selected energy regions representing ^{214}Pb, ^{212}Pb, and ^{40}K at 352, 239, and 1460 keV, respectively. Background count rates were measured using empty containers with the same geometry and dimensions at the same chosen regions of interest.

The radioactive concentrations (Ac) of ^{226}Ra, ^{22}Th, and ^{40}K in Bq/kg, which are contained in the studied samples were calculated using the following equation:[31,32]

$$Ac_{Ra,Th,or\ K} = \frac{C_s - C_b}{\epsilon \cdot I_\gamma \cdot M_s} \quad (1)$$

where the count rate measured at the chosen gamma line "regions of interest," C_s, (in count/s), the corresponding background count rate, C_b, (in count/s), the selected gamma line branching ratio, Iγ (%), the detector efficiency, ϵ (%), and the mass of the sample, M_s (kg).

2.2.2.2. Outdoor and indoor hazard indices and corresponding doses. Five parameters representing the outdoor radiological hazard indices and four parameters representing the indoor radiological hazard indices along with the corresponding doses/dose rates were derived from the measured activity concentrations of the main NORMs that exist in the studied samples. The aim is to investigate the maximum doses to be received upon external prolonged exposure to the materials under study besides those possible indoor doses upon staying for long in closed places constructed mainly from materials containing considerable amounts of the minerals understudy. The abovementioned hazard indices along with their associated descriptions, equations, safe limits, and references are stated in Table 1.

2.2.3. γ-ray attenuation measurements and derived shielding parameters

After performing the radiological hazard assessment, only four products were elected to investigate their radiation shielding properties against energetic photons.

2.2.3.1. Calculated effective atomic number. The effective atomic number (Z_{eff}), which indicates the electron cloud available to interact with the incident energetic photons and thus the attenuation capability of the shield against radiographs and γ-rays was computed using the computer program Auto-Z_{eff}, version 1.7.[33]

The mentioned program has a matrix of cross-sections at photons' energies ranging from 10 keV to 1 GeV for elements with atomic numbers equal to 1–100. The computed cross-sections for the composite shield, based on its elemental weight fractions, are compared with the built-in matrix as a function of Z, and then Z_{eff} is calculated at the specified energy by interpolation (b-spline) of Z values between the adjacent cross-sectional values.[33]

2.2.3.2. Experimental attenuation measurements. Six samples, for each product, were prepared through compression at 150 bar in a cylindrical mold to form a disk shape with a diameter of 2 cm and thickness of around 1 cm, as shown in Fig. 3, then the samples were coated with a very thin layer of polyvinyl alcohol to make the sample coherent and consistent.

Emitted γ-ray photons were counted and recorded versus the sample's thickness, to create the required transmission curves, at four different energies: 356, 662, 1173, and 1332 keV, which represent ^{133}Ba, ^{137}Cs, and ^{60}Co radioactive sources. Each measurement was taken for 600 s and corrected by subtracting the background measured under the same photo-peak. The experimental setup, shown in Fig. 4, was set based on the narrow-beam geometry. An inorganic scintillation detector with a 2′ × 2′ NaI(Tl) crystal was used for the measurements. The detector (model: 802-2M2/2 made by Canberra) is a hermetically sealed assembly consisting of a high-resolution crystal, a photomultiplier tube, conetic lined steel magnetic shield, an aluminum housing, and a 14-pin connector. A tube base (model: 2007P) which includes a preamplifier is connected to the photomultiplier tube to provide the operating bias that is derived from the Canberra 3002D high-voltage power supply. A LYNX 1024 Multi-Channel Analyzer with a color graphical display of spectra is used with the system and controlled using Genie 2000 software, Version 3.4.

The face of the detector was put in a cylindrical lead collimator; moreover, the detector, samples, and the radioactive source were all placed in a vertical alignment inside a lead chamber to ensure full protection against environmental and scattered radiation. A hollowed collimator of lead was placed over the source to achieve a narrow emitted bundle of γ-ray photons and improve the narrow-beam geometry. The dimensions of the source collimator are as follows: diameter, hollow internal diameter, and thickness are 3, 0.3, and 1 cm, respectively. The distance between the face of the detector and the source collimator was fixed at 7 cm.

2.2.3.3. Estimated shielding parameters. Based on the transmission curves obtained for the measured samples, linear attenuation coefficients (μ) in cm^{-1} at

Table 1. Outdoor and indoor hazard indices along with their details.

Hazard index	Description	Formula	Safe range	References
Outdoor hazard indices				
Radium equivalent activity (Ra_{eq})	An equivalent summed value gathering the specific activities of the main three NORMs: ^{238}U, ^{232}Th, and ^{40}K, as if they are all in terms of ^{226}Ra specific activity assuming that 370 Bq/kg of ^{226}Ra, 370 Bq/kg of ^{238}U, 259 Bq/kg of ^{232}Th, and 4810 Bq/kg of ^{40}K produce the same γ-ray dose rate	$Ra_{eq} = 370\left(\frac{Ac_{Ra}}{370}+\frac{Ac_{Th}}{259}+\frac{Ac_K}{4810}\right)$ (2)	Ra_{eq} <370 Bq/kg	(34,35)
Gamma index (Iγ)	A parameter that is used in evaluating construction and building materials to assess the possible γ-ray dose that may be obtained by dwellers or occupants who occupy places or buildings constructed mainly or partially from those materials.	$I_\gamma = \frac{Ac_{Ra}}{300}+\frac{Ac_{Th}}{200}+\frac{Ac_K}{3000}$ (3)	$I_\gamma \leq 1$	(19,36)
External hazard index (H_{ex})	H_{ex} is used mainly in this study to assess the possible external radiological exposure hazard upon being in direct and prolonged contact with the investigated materials which is the case of the workers who work in mining, separation, and piling up of these mineralogical materials.	$H_{ex} = \frac{Ac_{Ra}}{370}+\frac{Ac_{Th}}{259}+\frac{Ac_K}{4810}$ (4)	$H_{ex} \leq 1$	(35)
External absorbed dose rate ($\dot{D}_{out}$)	It is the rate by which the dose can be received during staying outdoor at 1 m above the ground level in an area that would be, in the current case, the mining, separation, and piling-up work sites, which contain significant amounts of the materials under investigation	$\dot{D}_{out} = 0.462Ac_{Ra} + 0.604Ac_{Th} + 0.0417Ac_K$ (5)		(35)
Outdoor annual effective dose (OAED)	Measures gamma dose that can be received outdoors due to NORMs. It depends on the occupancy factor T, which is a flexible factor that can be determined based on the time spent in the abovementioned working sites by the worker per year "taken as 1750 h/y"	$OAED = \dot{D}_{out} \times T \times F \times 10^{-6}$ (6)	OAED ≤1 mSv/y	(19,35)
Indoor hazard indices				
Alpha index (I_α)	I_α indicates that if its value exceeds unity then the activity concentration of ^{226}Ra in a building material exceeds 200 Bq/kg. Thus, indoor radon activity concentration exceeds 200 Bq/m^3, which results in exceeding the permissible internal accumulated dose, thus increasing the probability of getting lung cancer	$I_\alpha = \frac{Ac_{Ra}}{200}$ (7)	$I_\alpha \leq 1$	(19,20,37)
Internal hazard index (H_{in})	Adjusted for gamma rays and radon accumulation. The same factors are used like those used for predicting H_{ex}; however, the effect of ^{226}Ra becomes twice due to the emitted gamma rays and the possibility of receiving an internal dose that arises from the accumulation of radon in improperly ventilated areas.	$H_{in} = \frac{Ac_{Ra}}{185}+\frac{Ac_{Th}}{259}+\frac{Ac_K}{4810}$ (8)	$H_{in} \leq 1$	(19,35)
Internal absorbed dose rate ($\dot{D}_{in}$)	$\dot{D}_{in}$, in nGy/h, assumes that the dweller or the occupant is living in a standard room made entirely from the studied materials	$\dot{D}_{in} = 0.92Ac_{Ra} + 1.1Ac_{Th} + 0.08Ac_K$ (9)		(19,35,36)
Indoor annual effective dose (IAED)	Represents the possible indoor dose to be received assuming that the dweller spends about 80% of its day indoors so, the occupancy factor, T, will equal 7008 h/y	$IAED = \dot{D}_{in} \times 7008 \times 0.7 \times 10^{-6}$ (10)	IAED ≤1 mSv/y	(19,35,36)

NORMs, naturally occurring radioactive materials.

Fig. 3. Shape of samples used for the γ-ray attenuation measurements.

the studied γ-rays' energies were derived according to the Beer-Lambert equation as follows:[38]

$$\mu = \frac{1}{x} \times ln\left(\frac{I_0}{I_x}\right) \tag{11}$$

After that, the main shielding parameters were obtained based on the derived μ of the investigated samples. Thus, samples' shielding capabilities against γ-rays specifically at the studied energies were assessed through estimation of the required thicknesses, all measured in cm, to attenuate 50, 90, and ≃63% of the incoming γ-rays' photons referred to as half value layer, tenth value layer, and mean free path, respectively, according to the following equations:[18,38]

$$HVL = \frac{ln\,2}{\mu} \tag{12}$$

$$TVL = \frac{ln\,10}{\mu} \tag{13}$$

$$MFP = \frac{1}{\mu} \tag{14}$$

3. Results and discussion

3.1. Characterization of the studied samples

The investigated samples have been characterized by determining their chemical composition, real density, and particle size distribution, to obtain certain required preliminary information before proceeding with the main parts of the study, which consist of the assessment of the samples' radiological hazard impacts and γ-rays' shielding properties of the elected samples.

3.1.1. Chemical compositions and real densities

As mentioned previously, the sample's chemical composition and real density were determined using a BRUKER XRF Spectrometer and Ultrapyc 1200e Automatic Gas Pycnometer, respectively. The obtained results are tabulated in Table 2.

Based on the obtained results, all samples are found to have considerable percentages of heavy elements such as titanium (^{48}Ti), iron (^{56}Fe), and/or zirconium (^{91}Zr). High-Z elements are effective in

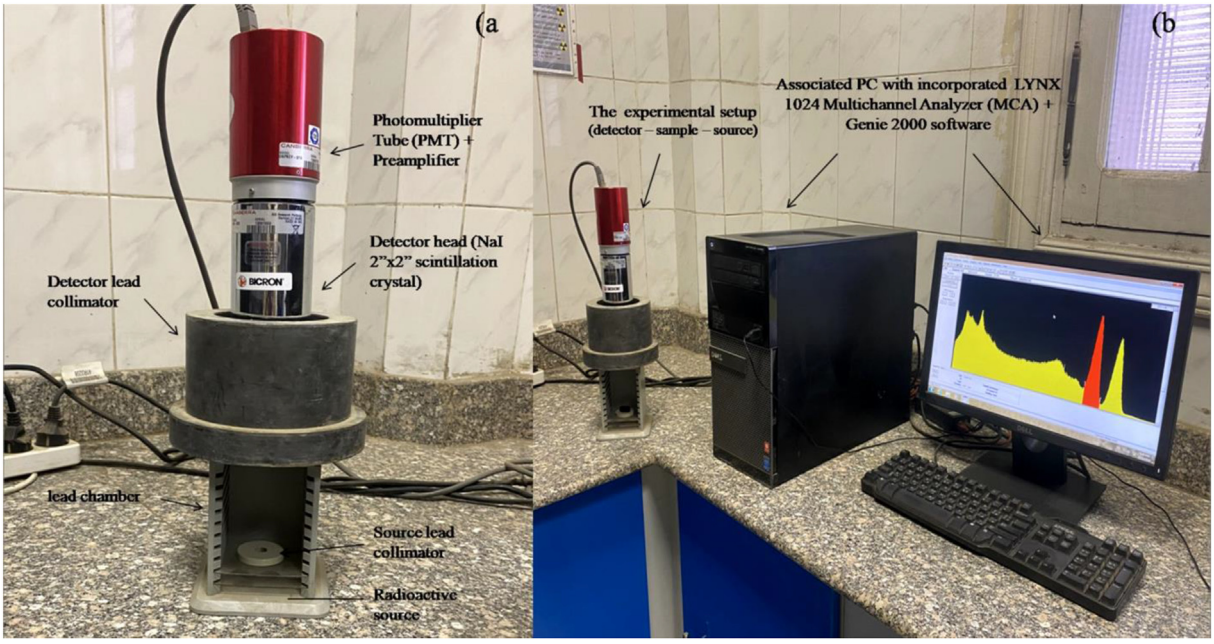

Fig. 4. Real photo for the experimental setup used during radiation attenuation measurements.

Table 2. Chemical composition and real density of the studied samples.

Oxide, %	Zircon	Ilmenite#1	BSC	Magnetite	Green silica	Rutile	Ilmenite#2
Na_2O	0.02	0.20	0.40	0.30	0.02	0.05	0.20
MgO	0.14	1.32	1.65	0.80	1.10	0.20	1.50
Al_2O_3	0.45	1.10	4.38	2.60	3.27	0.30	1.50
SiO_2	34.7	2.60	35.5	8.17	32.5	3.15	4.14
P_2O_5	0.56	0.10	0.20	0.12	0.01	0.05	0.11
SO_3	0.01	0.01	0.01	0.01	0.01	0.01	0.01
K_2O	0.04	0.20	0.60	0.30	0.12	0.04	0.20
CaO	1.60	1.80	7.10	2.12	6.00	0.40	2.50
TiO_2	0.91	43.3	17.8	18.8	29.7	79.8	42.2
MnO	0.03	0.90	0.50	0.40	0.14	0.12	0.80
Fe_2O_3	0.88	45.6	28.5	63.3	6.15	10.5	44.0
ZrO_2	58.4	0.01	1.50	0.11	18.2	3.00	0.11
PbO	0.41	0.42	0.09	0.51	0.62	0.60	0.39
Bi_2O_3	0.49	0.45	0.11	0.44	0.39	0.38	0.41
LOI	0.62	0.99	1.10	1.21	0.90	0.52	1.2
Density (g/cm^3)	5.228	4.675	3.638	5.018	3.864	4.443	4.603

Bi_2O_3, bismuth oxide; BSC, black sand concentrate.

attenuating energetic photons, such as radiographs and γ-rays. The three main interaction mechanisms of photons with matter are the photoelectric effect, Compton scattering, and pair production. All of these are directly proportional to the shield effective atomic number and density.[18,38] Speaking of density, all samples were found to be of high density. The zircon sample possessed the highest density, 5.228 g/cm^3, along with having a considerable amount of zirconium oxide, ZrO_2, which equals about 58%. Magnetite and Ilmenite grade no. 1 come after zircon; moreover, both samples have a variety of heavy elements. For instance, magnetite contains about 19 and 63% of TiO_2 and Fe_2O_3, respectively. However, it was found that the BSC sample possesses, comparatively, the lowest density and lowest content of high-Z elements.

3.1.2. Particle size distribution

Particle size distribution of the studied samples was analyzed, as mentioned before, using a BT-2001 particle size analyzer, which uses the laser diffraction technique. Both, cumulative percentage and difference percentage versus particle size were determined as shown in Figs 5 and 6, respectively.

Based on the obtained results, the samples' particle size was found to range between a few tens to a few hundreds of microns. For all studied samples, at least, 50% of particles are located between 100 and 200 μm and 90% of particles possess a particle size in the range of 50–200 μm. According to the estimated average particle size of the investigated samples, it was found to range from 101 μm, in the case of the ilmenite#1 sample, to 138 μm, in the case of the green silica sample, as presented in Fig. 7.

The relatively small particle size of the samples allows them to be used as additives to building materials or to be used as a percentage of fine aggregate in concrete, as it can improve the microstructure of the cementitious composite and thus its mechanical properties.[39,40] Also by

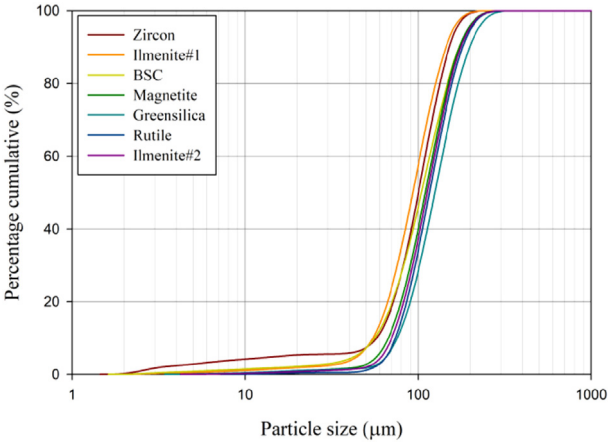

Fig. 5. Cumulative weight percentage of the studied samples.

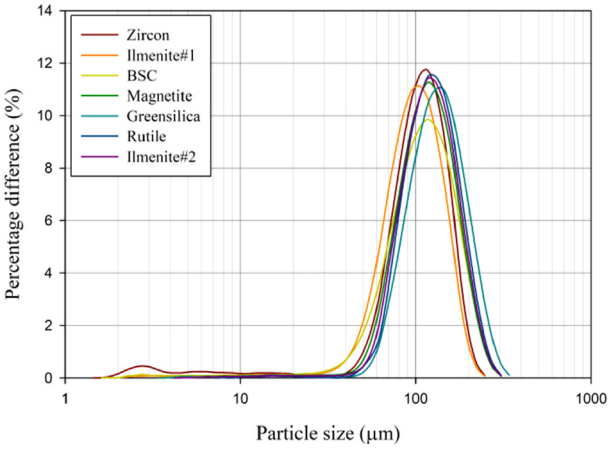

Fig. 6. Particle size distribution of the studied samples.

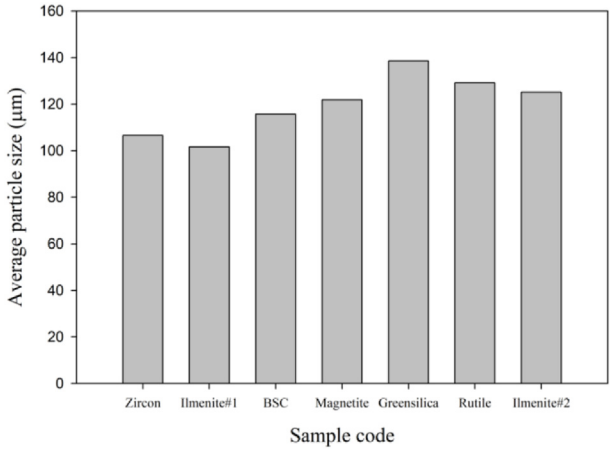

Fig. 7. Average particle size of the studied samples.

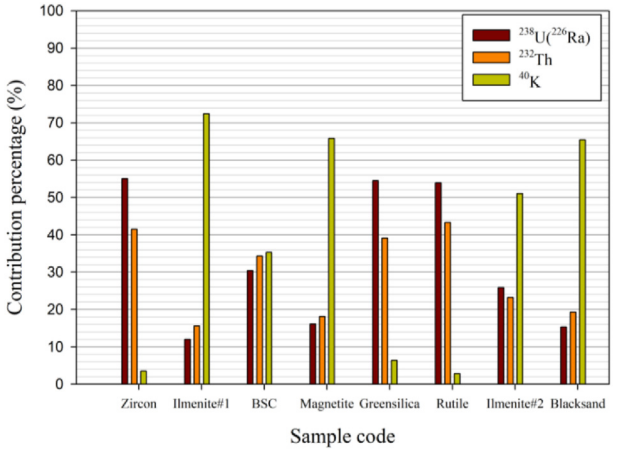

Fig. 8. Relative contributions to total activity concentrations due to ^{238}U (^{226}Ra), ^{232}Th, and ^{40}K for the studied samples including the reference black sand sample.

reducing the overall porosity and enhancing the packing density of the composite shield, the attenuation capability, especially against energetic photons, would increase.[18,40]

3.2. Specific activity and radiological hazard indices

3.2.1. Specific activities

Specific activities of the main naturally occurring radionuclides measured in the investigated samples along with their concentrations are given in Table 3.

The average activity concentrations of NORMs found in the Egyptian black sand, which is the source ore of the studied mineral products under study, were taken from Abdel-Rahman and El-Mongy.[41]

Based on the obtained values, it was found that the rutile sample has the highest total specific activity of 4841 Bq/kg, then zircon and green silica samples come in the second and third places with net specific activities equal to 4231 and 1912 Bq/kg, respectively. The major contribution in the total specific activities of these samples, as shown in Fig. 8, is due to ^{238}U, in terms of ^{226}Ra, and then ^{232}Th.

The measured specific activities of ^{238}U (^{226}Ra) in rutile, zircon, and green silica are; 2609 ± 235, 2342 ± 198, and 1043 ± 95 Bq/kg, and those of ^{232}Th are 2097 ± 84, 1757 ± 71, and 747 ± 36 Bq/kg, respectively. As can be observed, the obtained values are far higher compared with the mean international activity concentrations in soil stated by the UNSECAR report,[35] which set these values as 35 and 30 Bq/kg for both ^{226}Ra and ^{232}Th, respectively, which does make sense as these mineral products are processed through concentration and separation from Egyptian black sand, which is considered as a potential source of some strategic materials such as uranium, thorium, iron, titanium, and some rare earth elements.

The measured values of ^{226}Ra and ^{232}Th for the abovementioned three samples are also much higher than the recommended permissible activity concentration of 50 Bq/kg, which has been set for both ^{226}Ra and ^{232}Th in typical masonry.[35,36] However, the other studied samples magnetite, ilmenite#2, ilmenite#1, and BSC were found to have relatively low net specific activities ranging from 138.2 to 328.9 Bq/kg, even lower than that for natural black sand, 725.1 Bq/kg, from which those mineral

Table 3. Activity concentrations of the naturally occurring radioactive materials in the studied samples.

Sample code	^{238}U (^{226}Ra) (ppm)	^{238}U (^{226}Ra) (Bq/kg)	^{232}Th (ppm)	^{232}Th (Bq/kg)	^{40}K (%)	^{40}K (Bq/kg)
Zircon	211 ± 16	2342 ± 198	435 ± 17	1757 ± 71	0.42 ± 0.02	132 ± 5.28
Ilmenite#1	2 ± 0.16	22.21 ± 2.1	7.1 ± 0.4	29 ± 1.41	0.43 ± 0.02	135 ± 6.75
BSC	9 ± 0.81	99.9 ± 9.99	28 ± 0.98	113 ± 3.9	0.37 ± 0.01	116 ± 3.48
Magnetite	2 ± 0.17	22.2 ± 2.12	6.2 ± 0.3	25 ± 1.16	0.29 ± 0.01	91 ± 4.551
Green silica	94 ± 7.7	1043 ± 95	185 ± 8.9	747 ± 36	0.39 ± 0.02	122 ± 6.11
Rutile	235 ± 19	2609 ± 235	519 ± 21	2097 ± 84	0.43 ± 0.02	135 ± 6.75
Ilmenite#2	4 ± 0.35	44.4 ± 4.31	10 ± 0.41	40 ± 1.65	0.28 ± 0.01	88 ± 3.141
Black sand	10 ± 2.2	111 ± 24.5	34 ± 5.41	140 ± 22	1.51 ± 0.11	474 ± 36.3

BSC, black sand concentrate.

products have been extracted. They also possess NORM activity concentrations lower or close to the average international values in soil except for the BSC sample, which has higher ^{238}U (^{226}Ra)-specific and ^{232}Th-specific activities.

The specific activity of ^{40}K contained in the seven mineral products was found to be lower than that for natural black sand and the mean international value in soil, 400 Bq/kg[19,35] as the majority of potassium salts are usually removed during the concentration and separation processes.

3.2.2. Outdoor radiological hazard indices and doses

Based on the measured activity concentrations in the studied samples, the outdoor radiological hazard indices and the associated doses/dose rates are calculated and tabulated as presented in Table 4.

Considering the radium equivalent activity (Ra_{eq}) values estimated for the studied mineral products, the three samples that possess the highest "NORMs" activity concentrations were found to have the highest (Ra_{eq}) values much higher than the recommended maximum limit that equals 370.[19,31,35] Having (Ra_{eq}) value greater than the recommended maximum limit usually leads to a high outdoor dose rate (D'_{out}) and an outdoor annual effective dose (OAED) higher than the permissible dose to the public, which equals 1 mSv/y, upon exposure to external radiation. The high OAED values obtained for the abovementioned three samples show the mentioned positive correlation between Ra_{eq}, D'_{out}, and OAED. The three samples rutile, zircon, and green silica were found to exceed the maximum permissible annual dose with values equal to 3.04 ± 0.20, 2.64 ± 0.17, and 1.15 ± 0.08, respectively, which may cause unsafe consequences for the public or even for the workers who do not take the necessary radiation protection considerations upon prolonged existence in places containing these materials such as work sites, which contain piles of these products or buildings constructed mainly from these products.

However, the other four studied samples in addition to the reference black sand sample show acceptable (Ra_{eq}) values below the recommended limit and safer annual doses of less than the "1 mSv/y" recommended permissible limit. In general, these four studied samples, ilmenite#1, magnetite, BSC, and ilmenite#2, were found to have adequate and safe values for all outdoor radiological hazard indices and doses.

As predicted, rutile, zircon, and green silica samples greatly exceed the permissible "unity" value for both the gamma index ($I\gamma$) and the external hazard index (H_{ex}), which suggests the complete prevention of using the three mentioned mineral products as additives or alternative building materials even though their high densities and high-Z elements content nominate them to possess adequate shielding capabilities, especially against energetic photons. Also, the BSC sample shows a $I\gamma$ value slightly higher than unity, $I\gamma$ (BSC) = 1.22, which prevents the use of this material in construction materials as bulk amounts; however, it can be used on a smaller scale like in partial construction uses.

3.2.3. Indoor radiological hazard indices and doses

Based on the measured activity concentrations in the investigated samples, the indoor radiological hazard indices and the associated doses/dose rates are calculated and tabulated as shown in Table 5.

Considering the alpha and the internal hazard indices, as denoted before, both indices related directly to the possible risk due to the accumulated activity concentration of radon (^{222}Rn), especially in closed improperly ventilated spaces; thus, the possible indoor dose that may be received by the dwellers or the occupants. The main health concern that may arise from direct and prolonged inhalation of ^{222}Rn is the increased observed risk of lung cancer.[19,20,23]

To be on the safe side from the radiological protection point of view, both indices should be less than unity. Again, the three mineral products that

Table 4. Outdoor radiological hazard indices calculated for the studied samples.

Sample code	Outdoor hazard indices and doses				
	Ra_{eq}	$I\gamma$	H_{ex}	D'_{out}	OAED
	<370	≤1	≤1	(nGy/h)	(mSv/y)
Zircon	4865 ± 299	16.6 ± 1.02	13.1 ± 0.81	2149 ± 134	2.64 ± 0.17
Ilmenite#1	73.6 ± 4.64	0.26 ± 0.02	0.20 ± 0.01	33.2 ± 2.11	0.04 ± 0.00
BSC	270.6 ± 16	0.94 ± 0.05	0.73 ± 0.04	119.3 ± 7.1	0.15 ± 0.01
Magnetite	65 ± 4.129	0.23 ± 0.01	0.18 ± 0.01	29.2 ± 1.87	0.04 ± 0.00
Green silica	2121 ± 147	7.26 ± 0.49	5.73 ± 0.39	938.6 ± 66	1.15 ± 0.08
Rutile	5617 ± 356	19.2 ± 1.21	15.2 ± 0.96	2477 ± 159	3.04 ± 0.20
Ilmenite#2	108.9 ± 6.9	0.38 ± 0.02	0.29 ± 0.02	48.6 ± 3.12	0.06 ± 0.00
Black sand	347.1 ± 53	1.22 ± 0.18	0.94 ± 0.14	156 ± 23.71	0.19 ± 0.03

BSC, black sand concentrate; OAED, outdoor annual effective dose.

Table 5. Indoor radiological hazard indices calculated for the studied samples.

Sample code	Indoor hazard indices and doses					
	I_α	H_{in}	$D_{in(100\%)}$	$IAED_{(100\%)}$	$D_{in(26\%)}$	$IAED_{(26\%)}$
	≤1	≤1	nGy/h	mSv/y	nGy/h	mSv/y
Zircon	11.7 ± 0.99	19.5 ± 1.35	4098 ± 261	20.1 ± 1.28	1065 ± 67	5.23 ± 0.33
Ilmenite#1	0.11 ± 0.01	0.26 ± 0.02	62.7 ± 4.02	0.31 ± 0.02	16.3 ± 1.1	0.08 ± 0.01
BSC	0.50 ± 0.05	1.00 ± 0.07	225.6 ± 14	1.11 ± 0.07	58.6 ± 3.6	0.29 ± 0.02
Magnetite	0.11 ± 0.01	0.24 ± 0.02	55.2 ± 3.59	0.27 ± 0.02	14.3 ± 0.9	0.07 ± 0.01
Green silica	5.22 ± 0.47	8.55 ± 0.65	1792 ± 127	8.79 ± 0.63	466.1 ± 33	2.29 ± 0.16
Rutile	13.0 ± 1.18	22.2 ± 1.59	4717 ± 309	23.1 ± 1.52	1226 ± 80	6.01 ± 0.39
Ilmenite#2	0.22 ± 0.02	0.41 ± 0.03	92.3 ± 6.03	0.45 ± 0.03	23.9 ± 1.6	0.12 ± 0.01
Black sand	0.55 ± 0.11	1.23 ± 0.18	293 ± 45.1	1.44 ± 0.22	76.2 ± 11	0.37 ± 0.06

BSC, black sand concentrate.

show high and inadequate outdoor radiological parameters, rutile, zircon, and green silica, were found to have significantly high values of I_α and H_{in}. The reference black sand sample was found to possess adequate (I_α) but slightly high (H_{in}) value that equals 1.23 ± 0.18. In contrast, the other four investigated samples, magnetite, ilmenite#1, ilmenite#2, and BSC, show adequate low values for both indices with I_α values ranging from 0.11 ± 0.01 to 0.50 ± 0.05 and H_{in} values ranging between 0.24 ± 0.02 and 1.00 ± 0.07.

Speaking of the possible indoor doses, rutile, zircon, and green silica samples would have significantly high dose rates and thus, unsafe indoor annual effective doses ranging between $IAED_{(100\%)}$ = 8.79 ± 0.63 and 23.1 ± 1.52 mSv/y, in case of use as bulk amounts like using as bricks for instance. Also, the $IAED_{(100\%)}$ values of BSC or black sand were found to slightly exceed the safe permissible maximum dose, 1 mSv/y, with $IAED_{(100\%)}$ values equal to 1.11 ± 0.07 and 1.44 ± 0.22, respectively.

Considering the partial use of the investigated materials such as using them as aggregates' replacement in concrete, both indoor dose rate, $D_{in(26\%)}$, and annual effective dose, $IAED_{(26\%)}$, were calculated upon using these ores as one-third of the aggregates used to prepare concrete with a traditional mix design.[18] The average weight percentage of these materials considering their specific gravities was found to be about 26% relative to the overall concrete mass. It was found that, again, rutile, zircon, and green silica samples were still inadequate to be used as building materials even in the indicated partial amounts.

However, and as a conclusion from this phase, the other four mineral products were found safe, from the radiological protection point of view, to be used as building materials in bulk or partial amounts; thus, these four samples were elected to be studied during the third phase to assess their shielding capabilities against energetic photons.

3.3. Gamma radiation shielding assessment

Based on the former characterization, four mineral products have been elected to be investigated during this phase. The four minerals are ilmenite grade no. 1 (ilmenite#1), ilmenite grade no. 2 (ilmenite#2), magnetite, and BSC. The calculated effective atomic numbers of the four minerals from 10 keV up to 1000 MeV are shown in Fig. 9. Moreover, those calculated values at the four gamma lines under study are tabulated in Table 6.

Knowing that Z_{eff} is attributed to photons' interaction mechanisms with matter, its value greatly varies with the energy of the incident photons. As a result, the highest Z_{eff} values are observed at the low energy range due to the major contribution of the photoelectric mechanism, which greatly depends on the atomic number (Z). The cross-section of the photoelectric effect (σ_{pp}) is proportional to Z^n, where that n varies from 4.5 to 5. However, for

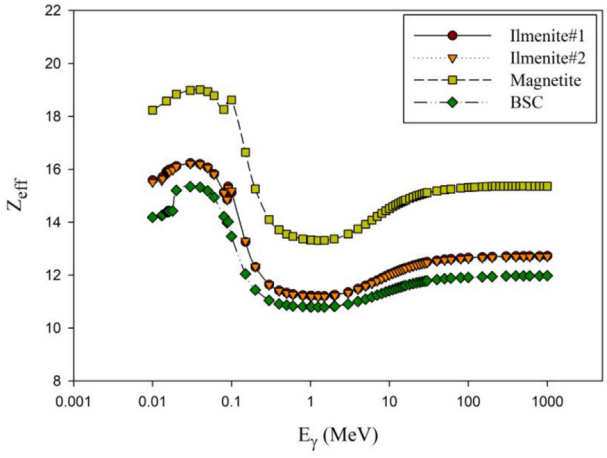

Fig. 9. Effective atomic number of the elected minerals as a function of photon's energy.

Table 6. Effective atomic number, Z_{eff}, for the elected minerals at four γ-rays' energies.

Eγ (keV)	Ilmenite#1	Ilmenite#2	Magnetite	BSC
356	11.54	11.50	13.84	10.97
662	11.27	11.25	13.42	10.82
1173	11.22	11.20	13.31	10.80
1332	11.21	11.18	13.30	10.79

BSC, black sand concentrate.

the intermediate energies, the lowest values can be observed due to the dominance of the Compton scattering mechanism, which is the least dependent on the shield's atomic number. After that, a reincrease in Z_{eff} values for all samples is noticed at the high energy range as the pair production mechanism, which depends on the squared value of the atomic number, becomes the primary interacting mechanism.[17,38]

Considering the vantage between the studied minerals, the magnetite sample was found to possess the highest Z_{eff} values over the entire energy range, which can be attributed to the significant heavy elements content such as titanium and iron, in contrast to BSC, which has the least content of the high-Z elements among the four investigated minerals.

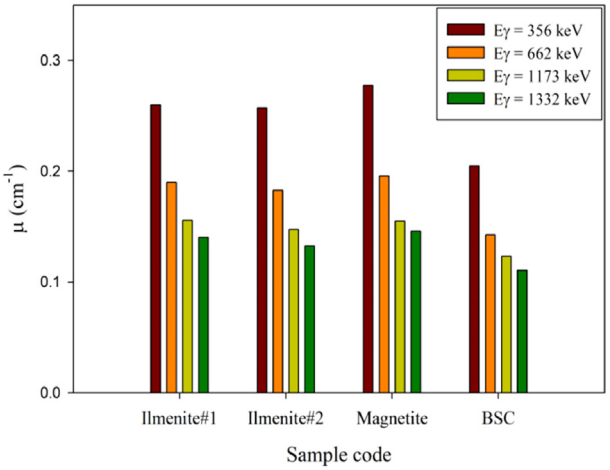

Fig. 11. Experimental linear attenuation coefficients for the studied samples at different energies.

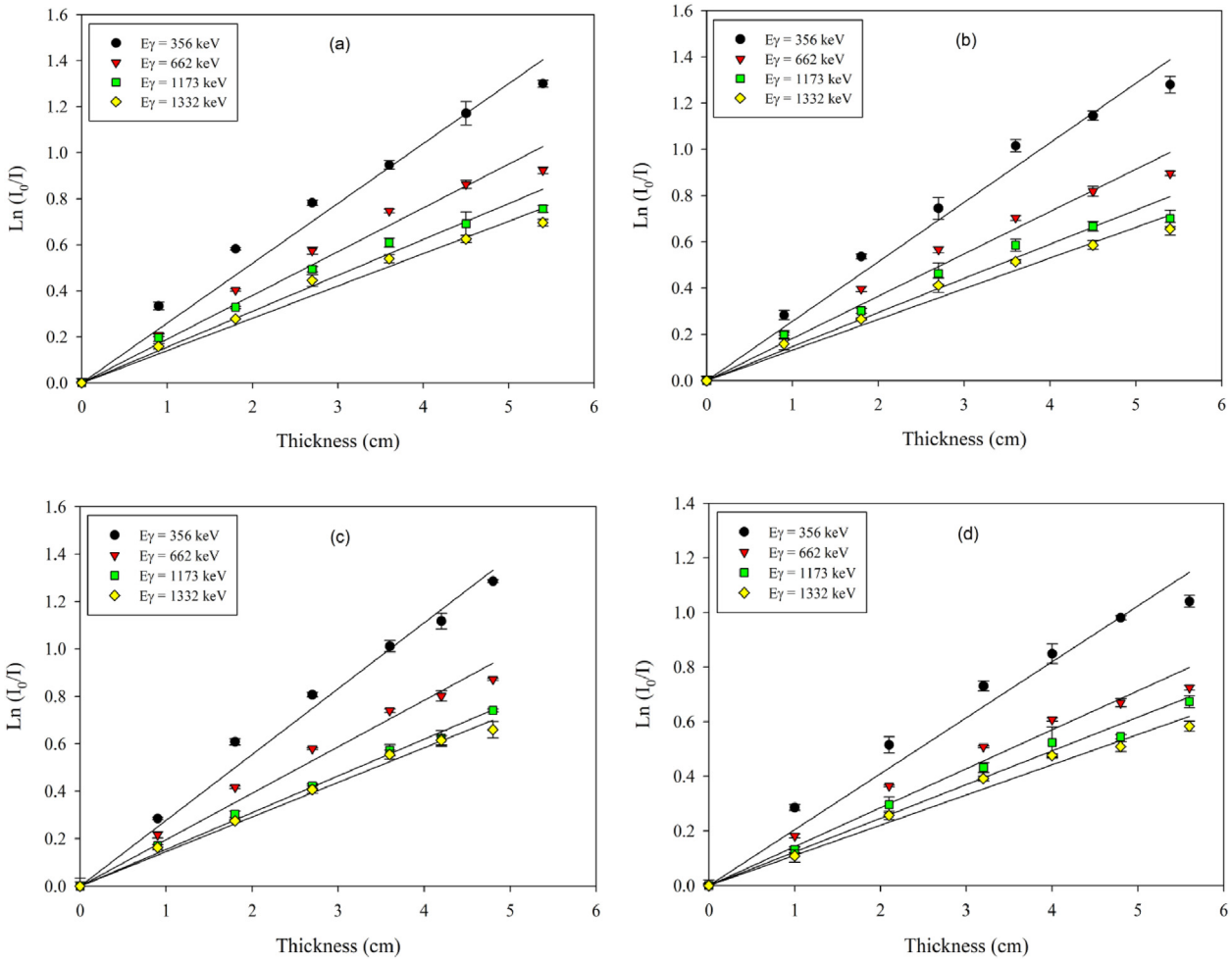

Fig. 10. Transmission curves at the studied energies for (a) ilmenite#1, (b) ilmenite#2, (c) magnetite, and (d) BSC. BSC, black sand concentrate.

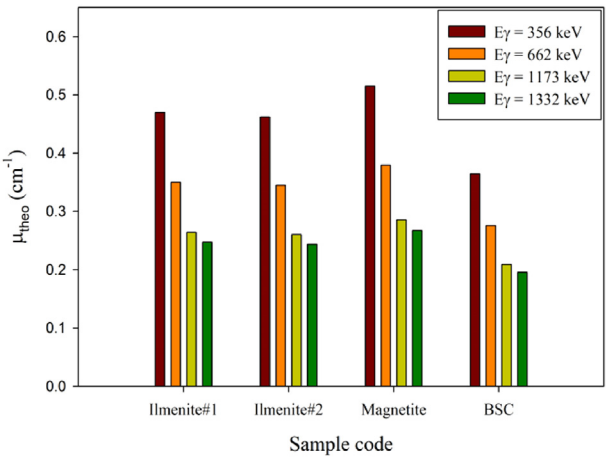

Fig. 12. Computed linear attenuation coefficients for the studied samples using the EpiXS software.

Based on the experimental γ-rays' attenuation measurements denoted before, the transmission curves have been obtained to derive the linear attenuation coefficients of the investigated samples at four different energies: 356, 662, 1173, and 1332 keV, which is attributed to ^{133}Ba, ^{137}Cs, and ^{60}Co radioactive sources. The obtained transmission curves are shown in Fig. 10.

The linear attenuation coefficients (μ), presented in Fig. 11, were obtained as the absolute value of the slope of the former transmission curves. It can be seen that (μ) decreases with the increase of the energy of the incident gamma photon which is logic as the main interaction mechanisms of photons with matter that dominates at the studied energies, photoelectric effect and Compton scattering, inversely proportion to the photon's energy. For further verification, the

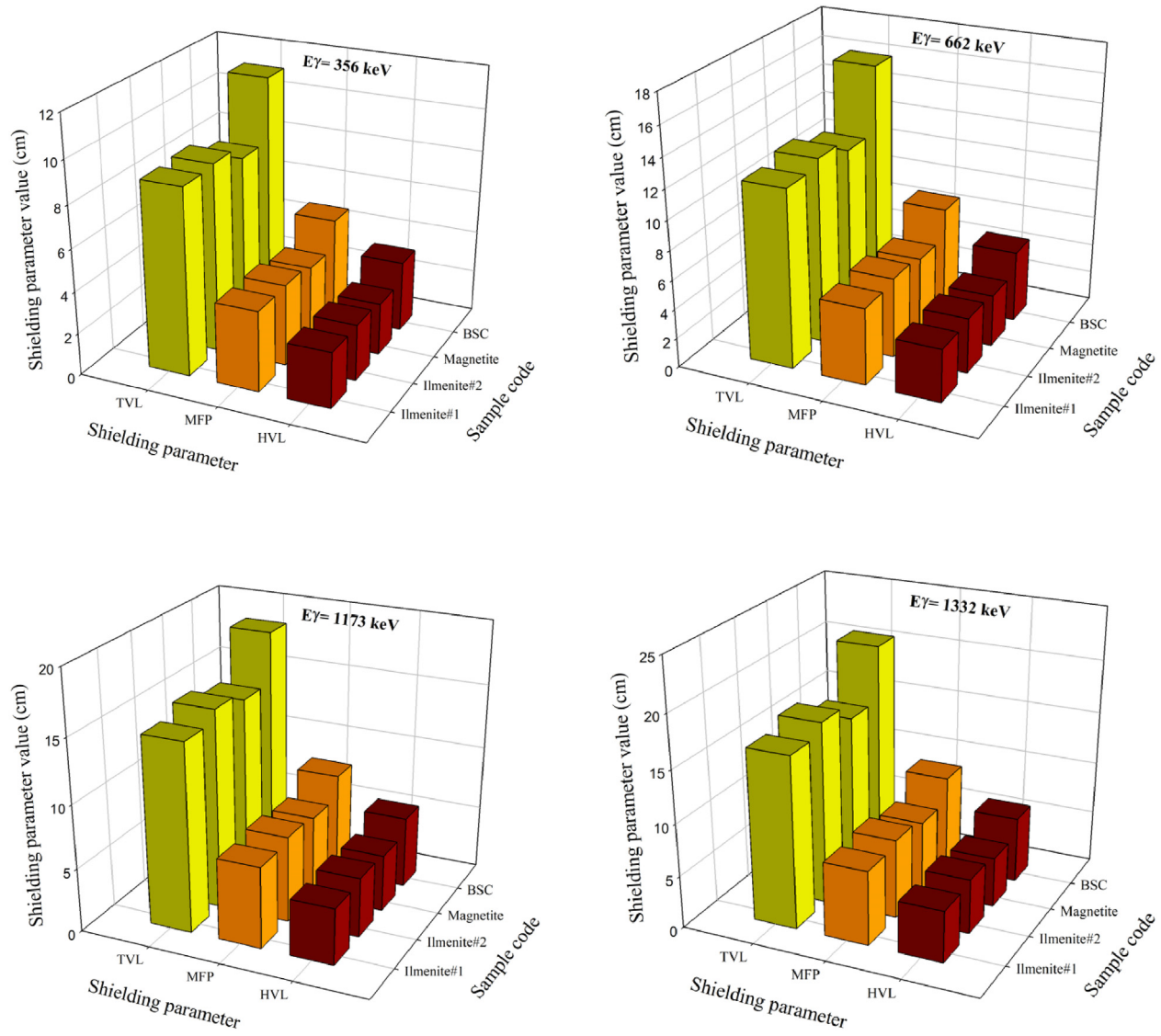

Fig. 13. HVL, TVL, and MFP of the studied minerals at the studied γ-rays' energies. HVL, half value layer; MFP, mean free path; TVL, tenth value layer.

theoretical linear attenuation coefficients at the same studied energies were computed for the four minerals, presented in Fig. 12, using EpiXS program, version 2.0.1. EpiXS is a Windows-based friendly user program that computes shielding parameters based on recently released built-in databases such as the ENDF/B-VIII database.

As the magnetite sample possesses the highest effective atomic number and the greatest density among the four studied minerals, it does make sense to have the highest (μ) values at the studied γ-rays' energies and vice versa. The BSC sample was found to have the least (μ) values because of its low density and small Z_{eff} compared with the other samples.

On comparing the obtained experimental linear attenuation coefficients to the computed ones, the same trend with the same preference among the studied samples can be observed which verifies the measurements. However, all the calculated μ values were found to be higher than their corresponding experimentally obtained ones. The reason is that the entries used by the software program are the exact chemical composition of the studied mineral alone along with its real density, but the representative disk samples that are used for the attenuation measurements are (a) coated with a thin layer of polyvinyl alcohol for consistency and (b) there was always an amount of air incorporated in the disk sample itself and between the vertically aligned samples during the measurements. The former can be considered a rational explanation for the observed differences between the experimentally obtained and the analytically calculated linear attenuation coefficients.

Based on these results, and as the shield thickness is a function of its linear attenuation coefficient (μ), the half value layer, tenth value layer, and mean free path, which are the required thicknesses to attenuate, 50, 90, and around 67% of the incoming photons,[17,38] respectively, were found to increase with the incident photon's energy, as shown in Fig. 13. Also, shielding thicknesses were found the lowest for magnetite and the highest for BSC, which is compatible with the obtained (μ) values.

4. Conclusions

Seven mineralogical products obtained from Egyptian black sand were investigated in this study. Physical, radiological, and radiation shielding characterization were carried out to assess the possibility of using these minerals in the production of building materials to improve their radiation shielding capabilities, especially against gamma rays. Based on the performed studies, the following major conclusions have been deduced:

(1) All minerals were found to possess high densities and their particle size lies in the microscale.
(2) All samples have notable percentages of high-Z elements knowing that zircon comes in the first place having the highest content of heavy elements and the greatest density and then magnetite and ilmenite grade no. 1 come in the second and third places, respectively.
(3) By measuring the activity concentration of the investigated samples due to their content of NORMs, three minerals proved to have significantly higher specific activities than the others. These three samples are rutile, zircon, and green silica.
(4) Based on the obtained outdoor and indoor radiological hazard indices, the abovementioned three minerals were found radiologically hazardous and can cause external and internal annual doses higher than the permissible limits recommended for the public. Moreover, their use in construction materials as bulk amounts or even as partial additions cannot be accepted. Thus, only the other four minerals were elected to investigate their γ-rays' shielding properties.
(5) The obtained γ-rays' shielding parameters indicate that magnetite and then ilmenite grade no. 1 both have promising shielding capabilities against energetic photons. These shielding capabilities along with the safe radiological indices obtained for both minerals encourage using them in construction materials if the radiation shielding properties are of importance.

Ethics standards

The manuscript complies with ethical standards.

Funding

No funding to be declared by the authors.

Conflict of interest

The authors declare that they have no conflict of interest.

Financial or non-financial interests

The authors have no relevant financial or non-financial interests to disclose.

References

1. Shultis JKX, Faw RE. Radiation shielding technology. *Health Phys*. 2005;88:297–322.
2. El-Samrah MG, Tawfic A, Chidiac SE. Spent nuclear fuel interim dry storage; design requirements, most common methods, and evolution: a review. *Ann Nucl Energy*. 2021;160:108408.

3. Halimah MK, Azuraida A, Ishak M, Hasnimulyati L. Influence of bismuth oxide on gamma radiation shielding properties of boro-tellurite glass. *J Non-Cryst Solids*. 2019;512:140–147.
4. Elsafi M, El-Nahal MA, Sayyed MI, Saleh IH, Abbas MI. Effect of bulk and nanoparticle Bi2O3 on attenuation capability of radiation shielding glass. *Ceram Int*. 2021;47:19651–19658.
5. Khazaalah TH, Shahrim I, Sayyed MI, Abdul Rahman A. Development of novel transparent radiation shielding glasses by BaO doping in waste soda lime silica (SLS) glass. *Sustainability*. 2022;14:937.
6. Hemath M, Sanjay MR, Dhakal HN, Kushvaha V. A comprehensive review on mechanical, electromagnetic radiation shielding, and thermal conductivity of fibers/inorganic fillers reinforced hybrid polymer composites. *Polym Compos*. 2020;41:3940–3965.
7. More CV, Alsayed Z, Badawi MS, Thabet AA, Pawar PP. Polymeric composite materials for radiation shielding: a review. *Environm Chem Lett*. 2021;19:2057–2090.
8. Tellili B, Elmahroug Y, Souga C. Investigation on radiation shielding parameters of cerrobend alloys. *Nucl Eng Technol*. 2017;49:1758–1771.
9. Levet A, Kavaz E, Özdemir Y. An experimental study on the investigation of nuclear radiation shielding characteristics in iron-boron alloys. *J Alloys Compd*. 2020;819:152946.
10. Alshahrani B, Olarinoye IO, Mutuwong C, et al. Amorphous alloys with high Fe content for radiation shielding applications. *Radiat Phys Chem*. 2021;183:109386.
11. El-Samrah MG, Abdel-Rahman MA, El Shazly R. Effect of heating on physical, mechanical, and nuclear radiation shielding properties of modified concrete mixes. *Radiat Phys Chem*. 2018;153:104–110.
12. El-Samrah MG, Abdel-Rahman MA, Kany AM. Study characteristics of new concrete mixes and their mechanical, physical, and gamma radiation attenuation features. *Z Anorg Allg Chem*. 2018;644:92–99.
13. Sallam FH, El-Samrah MG, Omar A, Tawfic AF, El Sayed AF. Enhanced bentonite/PVA matrix for advanced shielding applications. *Nucl Technol*. 2022;208:1666–1680.
14. Ali MA, Tawfic A, Abdelgawad MA, Mahdy M. Gamma and neutrons shielding using innovative fiber reinforced concrete. *Progr Nucl Energy*. 2022;145:104133.
15. Ali MA, Tawfic A, Abdelgawad MA, Mahdy M. Potential uses of different sustainable concrete mixtures in gamma and neutrons shielding purposes. *Progr Nucl Energy*. 2023;157:104598.
16. Kharita M, Takeyeddin M, Alnassar M, Yousef S. Development of special radiation shielding concretes using natural local materials and evaluation of their shielding characteristics. *Progr Nucl Energy*. 2008;50:33–36.
17. El-Samrah MG, Abreu Zamora MA, Novog DR, Chidiac SE. Radiation shielding properties of modified concrete mixes and their suitability in dry storage cask. *Progr Nucl Energy*. 2022;148:104195.
18. Kaplan MF. *Concrete Radiation Shielding*. United States: John Wiley and Sons Inc; 1989.
19. Ali M, Qureshi A, Waheed A, et al. Assessment of radiological hazard of NORM in Margalla Hills limestone, Pakistan. *Environm Monit Assess*. 2012;184:4623–4634.
20. Kocsis E, Tóth-Bodrogi E, Peka A, Adelikhah M, Kovács T. Radiological impact assessment of different building material additives. *J Radioanal Nucl Chem*. 2021;330:1517–1526.
21. Adelikhah M, Shahrokhi A, Chalupnik S, Tóth-Bodrogi E, Kovács T. High level of natural ionizing radiation at a thermal bath in Dehloran, Iran. *Heliyon*. 2020;6:e04297.
22. Dodge-Wan D, Viswanathan P. Terrestrial gamma radiation dose rate mapping and influence of building materials: a case study at Curtin University campus (Miri, Sarawak, Malaysia). *J Radioanal Nucl Chem*. 2021;328:163–180.
23. Khan AR, Mir KMR, Ur-Rahman R, Kearfott KJ. A review of radon measurement studies with nuclear track detectors (NTDs) in Azad Kashmir. *Indoor Built Environ*. 2017;26:447–455.
24. El-Kammar A, Ragab A, Moustafa M. Geochemistry of economic heavy minerals from Rosetta black sand of Egypt. *J King Abdulaziz Univ - Earth Sci*. 2011:2269–2297. http://dx.doi.org/10.4197/ear.22-2.4.
25. Abdel-Karim A-AM, Zaid SM, Moustafa MI, Barakat MG. Mineralogy, chemistry and radioactivity of the heavy minerals in the black sands, along the northern coast of Egypt. *J Afr Earth Sci*. 2016;123:10–20.
26. Mohamed TG, El-Midany AA, Ismael M, El-Samrah MG, Lotfy EA, Hassan MA. Risk assessment of radioactive hazards associated with black sand upgrading processes. *Appl Earth Sci*. 2023;132:187–193.
27. Mohamed TG, El-Midany AA, Ismael M, El-Samrah MG, Lotfy EA, Hassan MA. Effect of incorporating black sands (magnetite and ilmenite) into concrete mixtures on their mechanical properties. In: *5th Novel Intelligent and Leading Emerging Sciences Conference (NILES)*. IEEE; 2023. http://dx.doi.org/10.1109/NILES59815.2023.10296762.
28. El Aref M, Abd El-Rahman Y, Zoheir B, Surour AA. Mineral resources in Egypt (I): metallic ores. In: *The Geology of Egypt*. Switzerland: Springer; 2019:521–587.
29. García-Florentino C, Maguregui M, Fernández M, Queralt I, Margui E, Madariaga J. Usefulness of a dual macro-and micro-energy-dispersive x-ray fluorescence spectrometer to develop quantitative methodologies for historic mortar and related materials characterization. *Analytic Chem*. 2018;90:5795–5802.
30. Guerra VDG, Achiles AE, Béttega R. Influence of droplet size distribution on liquid dispersion in a Venturi scrubber: experimental measurements and CFD simulation. *Ind Eng Chem Res*. 2017;56:2177–2187.
31. Tawfic A, Awad HA, Zakaly M, Tantawy H. Natural radioactivity levels and radiological implications in the high natural radiation area of Wadi El Reddah, Egypt. *J Radioanal Nucl Chem*. 2021;327:643–652.
32. Turhan Ş, Baykan U, Şen K. Measurement of the natural radioactivity in building materials used in Ankara and assessment of external doses. *J Radiol Prot*. 2008;28:83.
33. Taylor M, Smith R, Dossing F, Franich R. Robust calculation of effective atomic numbers: the Auto-Zeff software. *Med Phys*. 2012;39:1769–1778.
34. Beretka J, Mathew PJ. Natural radioactivity of australian building materials, industrial wastes and by-products. *Health Phys*. 1985;48:87–95.
35. UNSCEAR. *Sources and Effects of Ionizing Radiation, United Nations Scientific Committee on the Effects of Atomic Radiation (UNSCEAR)*. New York, USA: United Nations; 2010.
36. European Commission, Directorate-General for Environment. *Environment, Radiological protection principles concerning the natural radioactivity of building materials*. Publications Office; 2000.
37. Bochicchio F. The newest international trend about the regulation of indoor radon. *Radiat Protect Dosim*. 2011;146:2–5.
38. Lamarsh JR. *Introduction to Nuclear Engineering*. third ed. Reading, MA, United States: Addison-Wesley Pub. Co.; 2001.
39. Berodier E, Scrivener K. Understanding the filler effect on the nucleation and growth of C-S-H. *J Am Ceram Soc*. 2014;97:3764–3773.
40. Chidiac SE, El-Samrah MG, Reda MA, Abdel-Rahman MAE. Mechanical, and radiation shielding properties of concrete containing commercial boron carbide powder. *Constr Build Mater*. 2021;313:125466.
41. Abdel-Rahman MAE, El-Mongy SA. Analysis of radioactivity levels and hazard assessment of black sand samples from Rashid area, Egypt. *Nucl Eng Technol*. 2017;49:1752–1757.